Stability of Polymer Ultrathin Films (<7 nm) Made by a Top-Down Approach

Jayanta Kumar Bal,[*,†,‡,#] Thomas Beuvier,[*,†,#] Aparna Beena Unni,[§] Elvia Anabela Chavez Panduro,[†,⊥] Guillaume Vignaud,[§] Nicolas Delorme,[†] Mohamed Souheib Chebil,[†,§] Yves Grohens,[§] and Alain Gibaud[†]

[†]LUNAM Université, IMMM, Faculté de Sciences, Université du Maine, UMR 6283 CNRS, Le Mans Cedex 9, 72000, France, [‡]Centre for Research in Nanoscience and Nanotechnology, University of Calcutta, Technology Campus, Block JD2, Sector III, Saltlake City, Kolkata, 700098, India, [§]Laboratoire d'Ingénierie des MATériaux de Bretagne, Centre de Recherche, Rue de Saint Maudé, BP 92116, 56321 Lorient Cedex, France, and [⊥]European Synchrotron Radiation Facility, BP 220, 38044 Grenoble Cedex, France. [#]J. K. Bal and T. Beuvier contributed equally.

ABSTRACT In polymer physics, the dewetting of spin-coated polystyrene ultrathin films on silicon remains mysterious. By adopting a simple top-down method based on good solvent rinsing, we are able to prepare flat polystyrene films with a controlled thickness ranging from 1.3 to 7.0 nm. Their stability was scrutinized after a classical annealing procedure above the glass transition temperature. Films were found to be stable on oxide-free silicon irrespective of film thickness, while they were unstable (<2.9 nm) and metastable (>2.9 nm) on 2 nm oxide-covered silicon substrates. The Lifshitz−van der Waals intermolecular theory that predicts the domains of stability as a function of the film thickness and of the substrate nature is now fully reconciled with our experimental observations. We surmise that this reconciliation is due to the good solvent rinsing procedure that removes the residual stress and/or the density variation of the polystyrene films inhibiting thermodynamically the dewetting on oxide-free silicon.

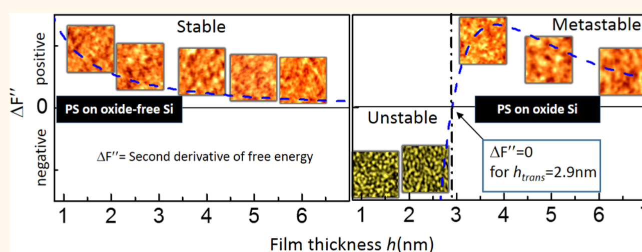

KEYWORDS: ultrathin film · stability · dewetting · adsorbed or residual film · solvent rinsing · free energy · Hamaker constant

The stability of thin polymer films is of paramount importance for a variety of applications such as sensors,[1] coating,[2] adhesives,[3] biomedical devices,[4] organic solar cells,[5,6] and organic thin-film transistors (OTFTs).[7] Despite a notably growing literature, it is not yet clear why polymer thin films often exhibit strong deviations from bulk behavior. For example, under certain conditions thin films show undesirable rupture, although they are expected to be energetically stable.[8] Key issues in interpreting these results are originating from sample preparation. The induction of residual stress during spin-coating due to out-of-equilibrium chain conformations that arise from rapid solvent loss has been frequently considered as the main source of instabilities.[9] It has been shown recently that the reduction of mechanical stresses can be achieved by severe thermal annealing for durations exceeding by far the reptation time.[10] However, when the film thickness becomes very small (typically on the order of a few R), numerous experiments show that annealing above the glass transition temperature (T_g) reveals their instability through the formation of holes. It is therefore of fundamental interest to address how one can predict the stability of a thin film and more importantly to propose a strategy for the stabilization of ultrathin films.

On the theoretical side, the Lifshitz−van der Waals intermolecular potential provides a convincing starting point for predicting the stability of a polymer thin film confined between two media. The free energy ΔF^{VDW} per unit area of a film of thickness h on a flat surface associated with this interaction can be written (up to a short-range repulsive term) as[11,12]

$$\Delta F^{VDW}(h) = \frac{-A_{Substrate/Film/Air}}{12\pi h^2} \quad (1)$$

Here, $A_{Subtrate/Film/Air}$ is the effective Hamaker constant of the three-layered component system (Substrate/Film/Air), which takes into account the substrate/film and the film/air interfaces. This expression does not consider the residual stress and the

* Address correspondence to jayanta.bal@gmail.com, tbeuvier@yahoo.fr.

Received for review April 21, 2015 and accepted July 6, 2015.

Published online July 06, 2015
10.1021/acsnano.5b02381

© 2015 American Chemical Society

density variations inside the films. The effective Hamaker constant can be expressed by the following mixing rule[11−14]

$$A_{\text{Substrate/Film/Air}} = A_{\text{Film/Film}} - \sqrt{A_{\text{Film/Film}} \times A_{\text{Substrate/Substrate}}} \quad (2)$$

with $A_{i/j}$ the Hamaker constants of materials i and j interacting across a vacuum. In the case of a polystyrene (PS) film deposited on a silicon (Si) wafer, it is found from the literature that the Hamaker constant of PS, $A_{PS/PS}$, is varying between 6.1 and 7.9 × 10^{-20} J,[12,15,16] while that of Si, $A_{Si/Si}$, is much higher (between 19 and 25.6 × 10^{-20} J[12−14,17] compared to that of silica, $A_{SiO2/SiO2}$ = 5.0 to 6.6 × 10^{-20} J[12,18−20]). Considering these values, it turns out that the Hamaker constant for flat interfaces of the system Si/PS/Air is negative, *i.e.*, $A_{Si/PS/Air} = -4.4$ to -6.0×10^{-20} J (using eq 2).

The sign of the Hamaker constant is crucial for determining the stability of a thin film.[21] When $A_{Sub/PS/Air} < 0$, the film is stable, while if $A_{Sub/PS/Air} > 0$, the film is unstable. Thus, if a PS film is attempted to be deposited on oxide-free Si, then the negative value of A should impose a stable film. Yet this is not the case, films usually dewet through hole nucleation. This inconsistency is generally interpreted either (1) by the existence of heterogeneities (*e.g.*, dust particles or defects) at the surface of Si, favoring a rupture called heterogeneous nucleation, or quite frequently (2) by the possible presence of a silica layer at the substrate−polymer interface, inducing a rupture called thermal nucleation or homogeneous nucleation, or (3) by spatial density variations due to film confinement, leading to variations in the Hamaker constants,[22] or (4) by the release of stress coming from the spin-coating preparation. Among these four hypotheses it is really difficult to choose the correct one because most of the time films encounter instability or metastability as soon as they are spin-coated. The underlying question that still remains open is the following one: Is it necessary to revise the theoretical approach or is it possible to preclude any of the possible causes for the dewetting?

Recently, Xue and Han[23] discussed the methods for inhibiting or slowing down the dewetting of polymer films. However, these approaches involve a change in the composition of the film (new end-groups, cross-linking agents, or additives) and are moreover difficult to set up for ultrathin films. In this context, we have explored a new strategy to inhibit the dewetting of ultrathin films without modifying the composition of the films. Inspired by the works of Koga,[24,25] Fujii,[26] and Napolitano,[10] who reported that thick polymer films can be thinned down after a good solvent rinsing, we have investigated the stability/instability behavior of PS films with tunable thicknesses ranging from ∼1.3 to 7.0 nm made on Si substrates with and without a native oxide layer following the top-down approach. We have observed that films on oxide-free Si substrates are stable after annealing above T_g, while films on an oxide (oxide layer thickness ∼2 nm) Si substrate are unstable (for film thickness h < 2.9 nm) or metastable (for h > 2.9 nm). These results, in agreement with the Lifshitz−van der Waals intermolecular theory, suggest that the good solvent rinsing procedure removes the residual stress and/or the density variations of PS films, hence inhibiting their dewetting.

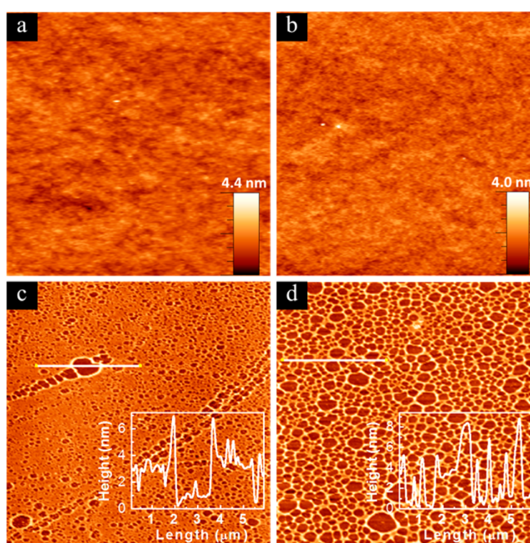

Figure 1. Wetting and dewetting of direct spin-coated PS films having different thicknesses. AFM images of PS films spin-coated at 2000 rpm on (a) SiO_x-Si and (b) H-Si surfaces from a 1.5 g/L solution (scan size = 5 × 5 μm²) and on (c) SiO_x-Si and (d) H-Si surfaces from a 0.75 g/L solution (scan size = 15 × 15 μm²). The thicknesses of the films determined by XRR are ∼6.8, 7.1, 3.2, and 4.3 nm for images (a), (b), (c), and (d), respectively. The insets of panels (c) and (d) correspond to the evolution of the height along the drawn line.

RESULTS AND DISCUSSION

Formation of Ultrathin Film (<7 nm) by Direct Spin-Coating. Let us first briefly report the general trends observed when a thin film of PS is deposited by spin-coating a very diluted solution (c < 1 g/L, where c stands for the concentration of PS in the toluene solution) on Si surfaces. Figure 1 shows AFM topographies immediately after depositing PS films by spin-coating dilute solutions at 2000 rpm. At c = 1.5 g/L and for higher concentrations films are perfectly smooth on both native oxide Si (labeled as SiO_x-Si) and oxide-free Si (labeled as H-Si) substrates (shown in Figure 1a and b, respectively). However, at c = 0.75 g/L (*i.e.*, 30 times less than the overlap concentration $c^* \approx 21$ g/L), films exhibit dewetting with a large number of randomly distributed holes, as shown in Figure 1c and d. The average thickness obtained from AFM (inset of Figure 1c and d) and also from X-ray reflectivity (XRR) (see Supporting Information Figure S1) is ∼3−4 nm.

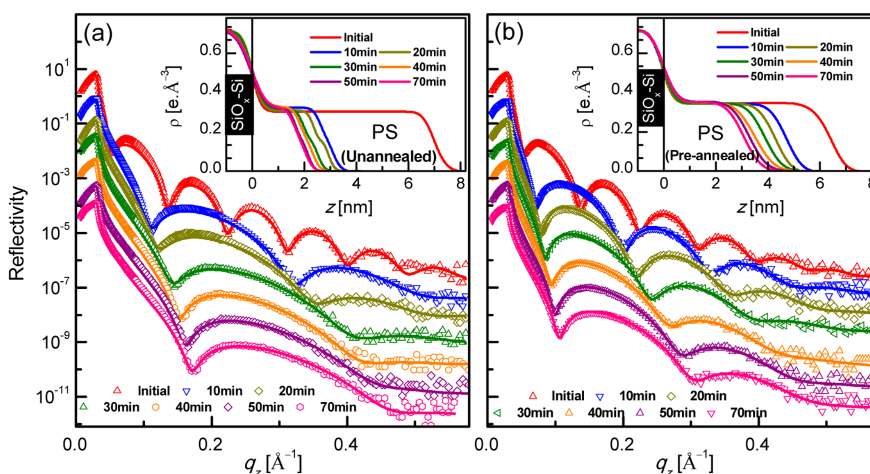

Figure 2. Structural evolution as a result of solvent rinsing. XRR data (symbols) and analyzed curves (solid line) of (a) unannealed and (b) preannealed 7 nm PS films on SiO_x-Si substrates before and after toluene rinsing during different durations (curves are shifted vertically for clarity). Insets: corresponding EDPs showing progressive decrement of the PS films thicknesses with toluene rinsing time.

The ruptures observed on the films made from diluted solutions cannot be explained by the van der Waals interaction according to the formalism mentioned in the introduction. It may probably come from residual stress during the fast evaporation of the solvent followed by a relaxation during the early stages of the film or from density heterogeneities. As a consequence, uniform ultrathin films of PS (M_w = 1.36 × 10^5 g/mol) with a thickness less than 7 nm are very difficult to obtain directly by spin-coating. The unexplained dewetting of thinner films on both Si surfaces together with the quest to produce uniform ultrathin films motivated us to adopt a new strategy.

Formation of Ultrathin Films (<7 nm) by Solvent Rinsing Treatment. Following the same leaching route as the one proposed by Guiselin *et al.*[27] and used by the research groups of Koga,[24,25] Tsui,[26] and Napolitano,[10] flat films of initial thickness equal to or greater than 7 nm were prepared by spin-coating both on oxide Si (SiO_x-Si) and oxide-free Si (H-Si) substrates (shown in Figure 1a and b). They were then sequentially immersed in toluene for 10 min and dried by mild flow of N_2 at ambient temperature and pressure. XRR data and the corresponding analyzed curves of pre- and postrinsing (up to 70 min of rinsing) for a PS film on SiO_x-Si are shown in Figure 2a. The Kiessig fringes for the 10 min rinsed film (blue curve) are well visible up to q_z = 0.45 Å^{-1}, highlighting a smooth surface (presumably no dewetting) and a film thickness close to 2.9 nm. According to the study of Koga's group,[24,25] we can assume that during this first rinsing the loosely attached layer was partly removed. This rinsing process was repeated several times on the same sample as shown in Figure 2a. As expected from ref 24, we observed that after the second rinsing the thickness decreased slowly. This decrement progressively increased upon further rinsing, and the film thickness reached about 1.7 nm after 70 min (*i.e.*, after 7 rinsings). We attributed this progressive decay of the film thickness to the desorption of the residual loosely attached layer. In contradiction with the work of Fujii *et al.*,[26] in which no residual film was found after just 30 min of toluene rinsing, the existence of a nonzero residual film even after "prolonged" toluene rinsing (see Supporting Information Figure S2) or when starting with a higher initial thickness ($h_0 \approx 130$ nm; see Supporting Information Figure S3) is a clear signature that an absorbed layer near the substrate/PS interface is already formed in the early times of spin-coating even though no annealing treatment has been performed. Our results correlate rather well with the observation of Napolitano *et al.*,[10] who have shown a nonzero adsorbed layer ($h_{ads}(t_{an} = 0) \neq 0$) (where t_{an} is the annealing time) without annealing. Johnson and Granick[28] estimated that the net segment–surface interaction energy between PS dissolved in carbon tetrachloride and an oxidized Si substrate is quite weak (∼1.3kT at 25 °C, where k is the Boltzmann constant and T is the absolute temperature) compared to that for PMMA (∼4kT). This weak interaction combined with the low segment–surface interaction number may explain why PS chains adsorbed at ambient temperature can desorb progressively in toluene with time. When films are annealed at 160 °C for 24 h before rinsing, called preannealed films, the decrement of thickness after the first rinsing is smaller, as shown in Figure 2b. The adsorption of PS segments initiated during the spin-coating is thus favored by annealing the samples above T_g, as reported by Napolitano *et al.*[10] and Jiang *et al.*[25]

A similar kind of behavior was also encountered in films grown on H-Si (see Supporting Information Figure S4). This confirms that annealing increases the thickness of the adsorbed layer as already reported[10,25] probably by enhancing the entanglement between

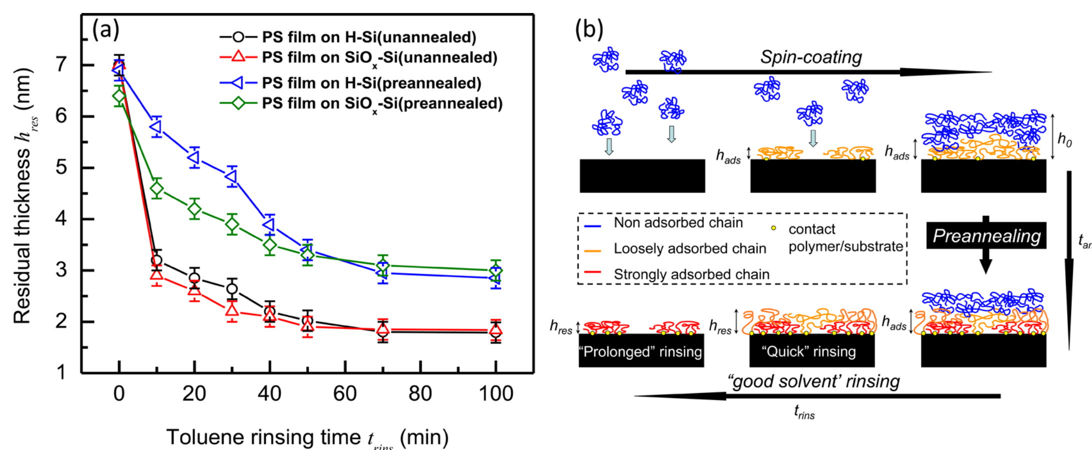

Figure 3. Correlation between the kinetics of dissolution and annealing. (a) Residual thickness (h_{res}) of preannealed and unannealed PS film of $h_0 \approx 7$ nm grown on SiO$_x$-Si and H-Si substrates as a function of rinsing time (t_{rins}). (b) Schematic illustration of the formation of an adsorbed layer h_{ads} during the spin-coating (prior to preparing a film of thickness h_0, shown in top panel) and preannealing (right panel) processes of PS film followed by toluene rinsing (bottom panel) that gives rise to a residual layer of thickness h_{res}. Preannealing incites the thickening of adsorbed layer h_{ads} and increases the number of polymer−surface interactions or contacts (labeled by small circle at the interface). Hence preannealed films exhibit a greater residual thickness h_{res} after toluene rinsing. Note that h_{ads} is equivalent to h_{res}. The two quantities differ only in the sense that h_{ads} corresponds to the thickness of the adsorbed layer before rinsing, whereas h_{res} corresponds to that of the adsorbed layer after rinsing, known as the residual layer.

the polymer chains and by increasing the number of segment−surface contacts with the substrate. Corresponding electron density profiles (EDPs) (shown in the inset of Figure 2a and b) show that the electron density of the film remains nearly constant to about 0.33 e/Å^3 (corresponding to a mass density of 1.02 g/cm^3 close to that of the bulk, 1.06 g/cm^3 [29,30]) for the unannealed samples and slightly higher for the preannealed films. The higher density for thin and annealed PS films was already reported.[31,32] In contrast to the work of Jiang *et al.*[25] and despite trying other density models, we were not able to prove that the adsorbed layer was composed of two layers with different densities coming from the loosely attached layer and a denser flattened layer. The best fits were obtained by using a single layer of PS with a constant density. The rinsing procedure may remove the density variation inside the film, or probing the existence of such a layer would need measurements at higher q wave vector transfers with high statistics. The thinnest good-quality residual films were found to be ~1.7 nm thick for unannealed films and ~2.9 nm thick for preannealed films after 70 min of toluene rinsing. From 100 min of rinsing, the quality of the films begins to deteriorate with an increase of the top surface roughness while the film thickness does not change appreciably (see Supporting Information Figure S2). One can thus infer that the loosely attached residual layer constituting the adsorbed layer is removed partially after 100 min of rinsing and completed after prolonged rinsing during 24 h. This observation is in agreement with Jiang *et al.*'s report.[25] Hence rinsing times (t_{rins}'s) less equal to 100 min were chosen for exploring the stability of such smooth ultrathin residual films presented in the second part of this paper. Additionally, we observed that in preannealed samples the adsorbed layer thickness obtained after 10 min of toluene rinsing was found to increase almost linearly with the radius of gyration (*e.g.*, R_g) of PS (see Supporting Information Figure S5). The relation $h_{ads} \approx 0.45 \times R_g$ (R_g ranging from 3 to 18 nm) was obtained, close to that obtained by Fujii *et al.*[25] for native-oxide-covered Si ($h_{ads} \approx 0.47\ R_g$), and confirms that the longer the PS chains, the thicker the adsorbed layer, as reported also by Housmans *et al.*[33]

The residual thickness (h_{res}) deduced from the fit of the XRR data is plotted in Figure 3a as a function of the rinsing time, t_{rins}. From this figure, it is evident that the film thickness can be controlled by tuning t_{rins}. A similar trend was witnessed by Gin *et al.*[24] A careful observation of Figure 3a reveals that h_{res} is higher for the H-Si supported preannealed PS film than for the SiO$_x$-Si supported one but only up to 40 min of rinsing. The difference for "quick" rinsed samples is in agreement with the work of Fujii.[26] For longer times, differences arise only when films are preannealed or not. The value of h_{res} for preannealed films is always greater than for unannealed films. For $h_0 \approx 7$ nm, after 70 min of toluene rinsing, h_{res} is found to be ~2.9 and ~1.7 nm for preannealed and unannealed films, respectively. During spin-coating, the adsorption process favors a transition from a chain's random-coil conformation in the solvent to a flat conformation on the substrate surface, as schematically illustrated in Figure 3b. It is accomplished by the diffusion of chains toward the interface.[10] Hence empty spaces should be there for incoming chains to attach with the substrate. For 7 nm thick films prepared from a solution of

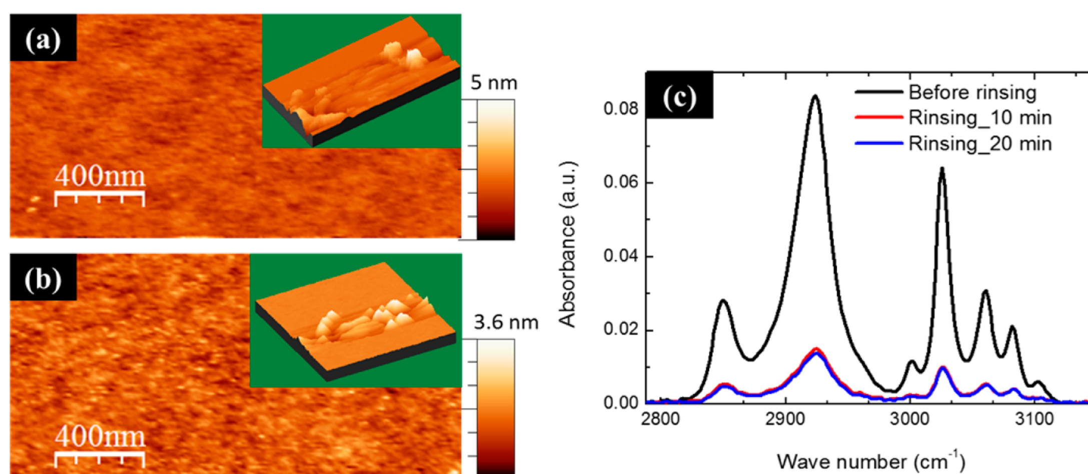

Figure 4. Morphology and verification of a residual layer on substrate surface. AFM topography image of preannealed residual films on (a) SiO_x-Si and (b) H-Si substrates obtained after 70 min of toluene rinsing. Insets of (a) and (b) show the 3D AFM images after scratching some regions of the residual film by the AFM tip in order to confirm that this is a polymer rather than Si substrate. (c) Attenuated total reflectance absorbance spectra of a PS ultrathin film before ($h_0 \approx 18.0$ nm) and after ($h_{ads} \approx 5.2$ nm) a "quick" toluene rinsing (up to 20 min), confirming the existence of a PS residual layer on the Si substrate.

concentration $c \approx 1.5$ g/L, one can expect flat conformations (shown in the top panel of Figure 3b) of adsorbed segments leading to a thin adsorbed layer (h_{ads}) as proposed by Napolitano *et al.*[10] The thickness of this layer is limited by the number of chains that are initially adsorbed at the interface. This layer is linked to the substrate (contact point is labeled by a small circle) and is difficult to remove by toluene rinsing. It probably determines the residual thickness (h_{res}) of the toluene-rinsed films. Annealing promotes the thickening of this adsorbed layer (shown in the right panel of Figure 3b) by providing more activation energy to fill more empty spaces at the polymer/Si interface. As a result, the chains reaching the surface in the later stages encounter a more crowded surface and can attach only by a reduced number of segments. Thus, a transition from a flat to a more vertical configuration takes place, which probably leads to a thicker residual layer (given by h_{res} in Figure 3a) in preannealed films. Surprisingly the electron density of the films remains nearly constant although the thickness is strongly reduced during the rinsing. This implies that the dissolution of polymeric chains is most likely occurring from the top surface, leaving the lower part unaffected.

AFM images depicting the surface morphology of these residual films after 70 min of toluene are shown in Figure 4a and b. Images show a smooth (RMS roughness <5 Å) and uniform residual PS film on both types of surfaces, such as on SiO_x-Si (Figure 4a) and H-Si (Figure 4b). In order to confirm that the observed topography comes from the soft polymer film and not from the Si surface, we scratched the surface of the film on both substrates by the AFM tip (shown in the insets of Figure 4a and b). We thus observed some patches of soft material, confirming the existence of a residual film on the Si surface.

It should be mentioned here that despite the application of high force (~2 nN) in the AFM scan prior to testing the existence of the residual film, we observe some patches instead of complete empty spaces through the scan area. It can be an indication that PS chains are strongly adsorbed to the substrate since when such a force is applied during scanning of soft materials, the bare substrate is generally observed after removing the soft film, as previously reported in the case of amphiphilic molecules grown on Si.[34] In addition, ATR spectroscopy was performed before and after toluene rinsing of an 18 nm (h_o) PS film grown on H-Si (shown in Figure 4c) to ascertain the presence of this residual film. Peaks located at 3000, 3030, 3060, 3085, and 3105 cm^{-1} are due to the C–H stretching modes of the C–H groups located in the benzene ring on the PS side chain. The bands with peak positions at 2930 and 2850 cm^{-1} are due to the C–H stretching vibration of the CH_2 and CH groups on the main PS chain, respectively.[35] The intensity of all the peaks decreases by about a factor of 4 after 10 min of toluene rinsing. This decrease is due to the removal of loosely attached PS chains during the rinsing. The thickness of the residual film obtained after 10 min of toluene rinsing (~5.2 nm) is also in agreement with the ATR results. Furthermore, beyond the first 10 min of toluene rinsing, the kinetics of dissolution drastically slows down (blue curve in Figure 4c), supporting the kinetics illustrated in Figure 3a. Hence this series of experimental results consistently confirms the existence of a residual PS layer and its kinetics on the substrate upon toluene rinsing.

Having proved that it is possible to produce uniform films of controlled thickness using this simple top-down approach by playing (1) on the nature of the substrate, (2) on the gyration radius of the polymer (R_g), (3) on the preannealing time (t_{an}), and (4) on the rinsing time (t_{rins}), we want to address now the stability of the rinsed PS

TABLE 1. Preparation of the PS Rinsed Films on Si Substrates (6 samples on H-Si and 6 samples on SiO_x-Si)[a]

sample name	silicon treatment	initial PS thickness h_0 (nm)	preannealing time t_{an} at 160 °C (h)	rinsing time t_{rins}(min)	residual PS film thickness h_{res} (nm)	stability after postannealing at 120 °C for 24 h
H-Si-a	HF	7	0	100	1.5	no dewetting
H-Si-b	HF	7	0	50	2.5	no dewetting
H-Si-c	HF	7	24	40	4.0	no dewetting
H-Si-d	HF	7	24	20	4.6	no dewetting
H-Si-e	HF	7	24	10	5.0	no dewetting
H-Si-f	HF	16	24	2	6.0	no dewetting
SiO_x-Si-a	RCA	7	0	100	1.3	dewetting
SiO_x-Si-b	RCA	7	0	50	1.7	dewetting
SiO_x-Si-c	RCA	7	0	30	2.2	dewetting
SiO_x-Si-d	RCA	7	0	10	3.5	no dewetting
SiO_x-Si-e	RCA	7	24	10	4.9	no dewetting
SiO_x-Si-f	RCA	16	24	1	6.8	no dewetting

[a] Preannealing time t_{an} of the film (before the rinsing procedure) and the duration of toluene rinsing t_{rins} determine the thicknesses of residual layer (h_{res}).

films when they are postannealed above T_g depending on the type of treatment of the Si substrate.

Stability or Instability of Residual Films of Tunable Thickness. The stability of thin films strongly depends on their thickness and on the chemical treatment of the Si substrate.[21] Therefore, 12 films were initially spin-coated on both SiO_x-Si (6 films) and H-Si (6 films) surfaces with thicknesses mostly (10 films) of 7 nm and few (2 films) of 16 nm prior to carrying out the rinsing. Films having different h_{res} values were thus obtained by varying either the rinsing time or the preannealing treatment as tabulated in Table 1. Their stability was then scrutinized after they were annealed (at 120 °C) above the T_g of bulk polystyrene. For the sake of clarity, this annealing treatment performed after rinsing is labeled as "postannealing". We first report the results obtained on H-Si before commenting those on SiO_x-Si.

Stability of Residual Films on H-Si Wafers. Let us recall that PS ultrathin films on H-Si wafers usually dewet the surface of the substrate (see Figure 1d), thus violating the prediction given by the Liftshitz–van der Waals theory. Our aim here was to test again if this violation was seen for a series of uniform films of different thicknesses having undergone a leaching treatment. Residual uniform films with thicknesses ranging from 1.5 to 6.0 nm were thus obtained on H-Si wafers (see Table 1) by tuning both the preannealing time of the films and the duration of toluene rinsing. The procurement of such uniform films is a "*sine qua non*" condition to apprehend their stability upon annealing. Indeed to apply physical models such as the one based on a Liftshitz–van der Waals interaction, it is compulsory to start with uniform films of known thickness (as shown by eq 1). The best way to probe the stability of such films is to perform AFM imaging of the surface of the residual PS films after postannealing above the T_g of bulk PS. Figure 5A shows such images for residual PS films of thickness ranging from ~1.5 to ~6.0 nm on H-Si after postannealing at 120 °C for 24 h. Further rise in the annealing temperature to 170 °C does not show any kind of dewetting (see Supporting Information Figure S6). In contrast to the directly spin-coated films (see Figure 1d), the leached films of identical thicknesses were found continuous and flat (see Figure 5A). No dewetting occurred in this case, thus reconciling our experimental observations with the prediction of the Liftshitz–van der Waals theory. With this in mind, it was natural to consider the behavior of films prepared in the same way but deposited on SiO_x-Si substrates.

Instability/Metastability of Residual Films on SiO_x-Si Wafers. AFM images of residual films with h_{res} in the range 1.3 to 6.8 nm on SiO_x-Si followed by postannealing at 120 °C during 24 h under vacuum are shown in Figure 5B. The results observed in this AFM study are in marked contrast with those obtained on H-Si substrates. AFM images of thinner films (h_{res} < 2.9 nm) shown in Figure 5Ba, b and c reveal a bicontinuous surface pattern.[36−38] For thicker films (h_{res} > 2.9 nm) shown in Figure 5Bd, e and f, we clearly observed a smooth, flat and continuous morphology. Therefore, there is a threshold in thickness of about 2.9 nm above which residual films (or adsorbed layer) remain stable. Below this threshold, the formation of bicontinuous structures can be understood in terms of spinodal dewetting.[36−38] In order to extract the characteristic features of these dewetted patterns, fast Fourier transform (FFT) of topographic images was conducted with results shown in the corresponding insets of each figure. In the case of spinodal dewetting, the FFT yielded ring patterns indicating the existence of a correlation peak consistent with a definite correlation length λ. A radial averaging of the FFT images or power spectral density (PSD) calculation (see Supporting Information Figure S7) of topographic images was then achieved to extract the value of $\lambda \approx 53-63$ nm. This value is comparable to the value reported by Seeman *et al.*[21] with low PS molar mass ($M_w = 2 \times 10^3$ g/mol).

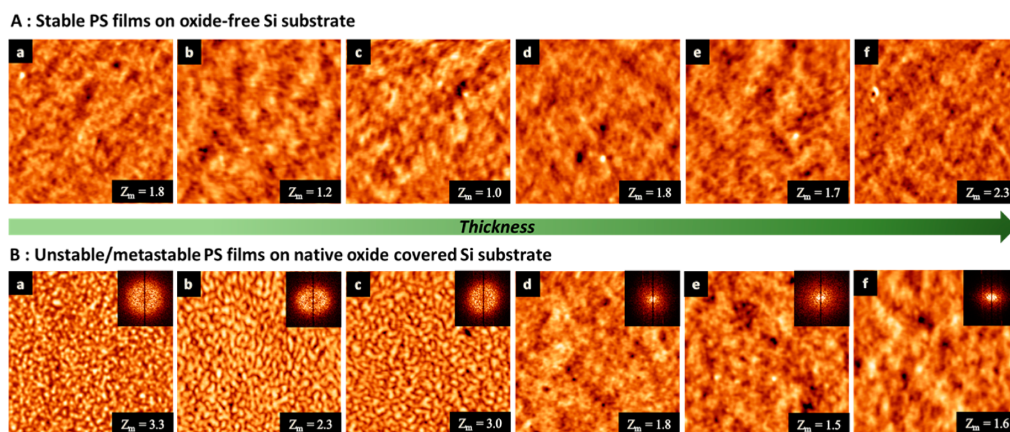

Figure 5. (A) Stability and (B) instability/metastability of residual PS films on oxide-free Si (H-Si) and on native-oxide-covered Si (SiO_x-Si), respectively. AFM topographic images (scan size = 1 × 1 μm^2) presented in the top panel (A) show the morphologies of residual films of thickness h_{res} (a) ≈ 1.5 nm, (b) ≈ 2.5 nm, (c) ≈ 4.0 nm, (d) ≈ 4.6 nm, (e) ≈ 5.0 nm, and (f) ≈ 6.0 nm on H-Si after postannealing. In the bottom panel (B) AFM images show similar results for h_{res} of (a) ≈ 1.3 nm, (b) ≈ 1.7 nm, (c) ≈ 2.2 nm, (d) ≈ 3.5 nm, (e) ≈ 4.9 nm, and (f) ≈ 6.8 nm thick films on SiO_x-Si. Inset shows their corresponding 2D FFT image. Morphologies were obtained after postannealing at 120 °C during 24 h. Note that the thicknesses that are mentioned here are the thicknesses of the residual films just before the postannealing. Z_m represents the maximum height in nm.

TABLE 2. Correlation between the Hamaker Constant Values of $A_{Si/Si}$, $A_{PS/PS}$, and $A_{SiOx/SiOx}$ and the Resulting Effective Hamaker Constants $A_{Si/PS/Air}$ and $A_{SiOx/PS/Air}$ from the "Mixing Rule" of eq 2,[a]

	$A_{Si/Si} \times 10^{-20}$ J	$A_{PS/PS} \times 10^{-20}$ J	$A_{SiOx/SiOx} \times 10^{-20}$ J	$A_{Si/PS/Air} \times 10^{-20}$ J	$A_{SiOx/PS/Air} \times 10^{-20}$ J	state of PS for d_{SiOx} = 2 nm
curve A	24.0	6.15	6.6	−6.0	−0.2	stable
curve B	19.0	7.9	5.0	−4.4	1.6	unstable
curve C	20.3	6.5	5.2	−5.0	0.7	unstable/metastable

[a] Curves A, B, and C refer to the three different states as shown in Figure 6.

No need to say that flat, featureless films studied by the same procedure did not show any correlation peak.

The full interpretation of such beautiful results can be once again obtained by the Lifshitz−van der Waals interaction potential. Yet, it is necessary to now consider the presence of the silicon oxide layer to explain our results. The system that needs to be considered is thus made of four media, Si/SiO_x/PS/Air, in which the thickness of the oxide layer is denoted d_{SiOx}. Application of eq 1 assuming pairwise addition leads to the following expression for the free energy:[40,41]

$$\Delta F^{VDW}(h) = \left(\frac{-A_{Si/PS/Air}}{12\pi(h+d_{SiO_x})^2}\right) + \left(\frac{-A_{SiO_x/PS/Air}}{12\pi h^2}\right) - \left(\frac{-A_{SiO_x/PS/Air}}{12\pi(h+d_{SiO_x})^2}\right) \quad (3)$$

where $A_{Si/PS/Air}$ and $A_{SiOx/PS/Air}$ are the effective Hamaker constants of the Si/PS/Air and the SiO_x/PS/Air systems, respectively.

The values of the Hamaker constants are not very well defined in the literature and are ranging from $A_{Si/PS/Air} = -4.4$ to -6.0×10^{-20} J and $A_{SiOx/PS/Air} = -0.22$ to 1.6×10^{-20} J. Substituting d_{SiOx} = 2 nm (see Supporting Information Figure S10) in the case of the SiO_x-Si substrate, $\Delta F^{VDW}(h)$ can vary considerably depending on the values of $A_{Si/PS/Air}$ and $A_{SiOx/PS/Air}$ (given in Table 2). For instance in Figure 6, we have plotted $\Delta F^{VDW}(h)$ with the values of the effective Hamaker constants given in Table 2. Curve A, which was calculated with $A_{Si/PS/Air} = -6.0 \times 10^{-20}$ J and $A_{SiOx/PS/Air} = -0.22 \times 10^{-20}$ J, corresponds to a stable state since the second derivate of the free energy is always positive. On the contrary, curve B, calculated with $A_{Si/PS/Air} = -4.4 \times 10^{-20}$ J and $A_{SiOx/PS/Air} = 1.6 \times 10^{-20}$ J, depicts an unstable state since the second derivative is always negative. The interpretation of a spinodal decomposition for $h < 2.9$ nm can be explained only if the variation of $\Delta F^{VDW}(h)$ would be similar to the one plotted in curve C. Curve C was obtained by adjusting the Hamaker constant to $A_{Si/PS/Air} = -5.0 \times 10^{-20}$ J and to $A_{SiOx/PS/Air} = 0.7 \times 10^{-20}$ J. Note that these values are almost in the middle range of the ones found in the literature. Additionally they dictate the value of the threshold thickness h_{trans} delimiting the unstable from the metastable zones. A dashed line shown in Figure 6 (right *y*-axis) shows the plot of the second derivative of the free energy, *i.e.*, $[\Delta F^{VDW}(h)]''$, corresponding to the C curve. For $h < 2.9$ nm, $[\Delta F^{VDW}(h)]'' < 0$, films are unstable and dewet as observed in the AFM images a, b, and c of Figure 5B. For $h > 2.9$ nm, $[\Delta F^{VDW}(h)]'' > 0$, films are metastable and do not dewet, as observed in the AFM images d, e,

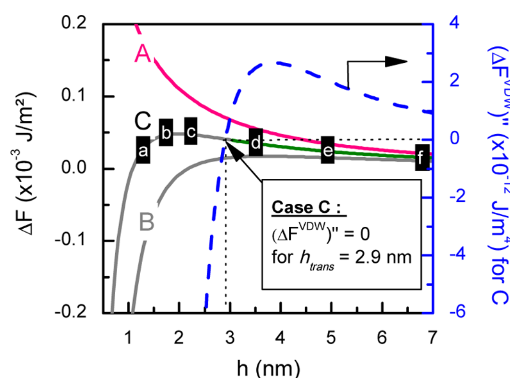

Figure 6. Evolution of the free energy as a function of film thickness with different sets of Hamaker constants. Simulated (solid lines) and (dashed line) curves using eq 3 considering 2 nm native oxides present on SiO_x-Si substrate. Curve A, drawn by choosing $A_{Si/PS/Air} = -6.0 \times 10^{-20}$ J and $A_{SiOx/PS/Air} = -0.2 \times 10^{-20}$ J, corresponds to a stable state. Curve B, deduced with $A_{Si/PS/Air} = -4.4 \times 10^{-20}$ J and $A_{SiOx/PS/Air} = 1.6 \times 10^{-20}$ J, depicts an unstable state. Curve C, plotted assuming $A_{Si/PS/Air} = -5 \times 10^{-20}$ J and $A_{SiOx/PS/Air} = 0.7 \times 10^{-20}$ J, corresponds to either a metastable state above $h_{trans} \approx 2.9$ nm or unstable films below h_{trans}. The letters a, b, c, d, e, and f correspond to the AFM images presented in Figure 5. Color of state: stable in pink, unstable in gray, metastable in green.

and f of Figure 5B. The threshold thickness h_{trans} = 2.9 nm corresponds to the zero value of the second derivative. Notably the thickness of the native oxide layer is found to be crucial for determining the h_{trans} value (see Supporting Information Figure S8). It has a linear dependency on the oxide thickness ($h_{trans} \propto d_{SiOx}$).

In the introduction of this paper, we mentionned that the behavior of polymer ultrathin films confined at the surface of chemically etched silicon was still a mystery. The underlying reason was that the most recognized theory utilized for predicting the stability of such films failed when films were deposited on oxide-free silicon surfaces. This issue was never solved, and it was natural to either question the validity of the theory or consider that one of the four stated hypotheses in the introduction section would be at the origin of observed phenomena. So far none of these possibilities could be ruled out. However, the validity of the Lifshitz−van der Waals interaction potential was difficult to distrust, and for this reason it was clear to us that the reconciliation between the theory and the experimental observation could come from a modification of the sample preparation. Following the stimulated route proposed by Koga,[24,25] Fujii,[26] and Napolitano[10] we are now confident that the first two hypotheses, *i.e.*, the dewetting due to heterogeneities or the presence of silica, can be excluded. Indeed, if there were any heterogeneities and/or an oxide layer on the Si surface causing the dewetting of directly spin-coated films, there should be no reason to get a stable residual film on H-Si after the leaching procedure. Also it is not feasible to assume that the oxide layer and the heterogeneities present at the dewetted PS film-Si interface would be removed by the rinsing treatment. Thus, the application of this novel technique narrowed the possible reasons for the common discrepancy between experimental results (Figure 1c and d) and theoretical expectations (eq 1). The two other hypotheses for the dewetting, *i.e.*, the stresses induced by the spin-coating procedure and/or density variation, could not yet be excluded. The leached films were then postannealed at 120 °C, and their stability was revisited. The observed results were then confronted with the theory in a very successful way since the behavior of PS films both on oxide-free and on SiOx silicon surfaces was fully explained. The good agreement between the observed domains of stability of the residual films and the underlying theory promotes the idea that the leaching route has removed residual stresses and/or local density variations originating from the spin-coating and from the fast evaporation of the solvent. Such stresses are usually considered to be at the origin of the dewetting of directly spin-coated PS films on both oxide-free (H-Si) and native-oxide-covered (SiO_x-Si) Si surfaces (as shown in Figure 1c and 1d). In contrast, the leached films of identical thicknesses are amazingly stable on the H-Si surfaces. One can thus conclude that the leaching procedure combined with a postannealing leads to stable films on H-Si substrates. In addition all residual films on H-Si were found to be stable at ambient conditions up to ∼2 months without postannealing (see Supporting Information Figure S9). Hence, one can infer that the toluene rinsing induces a chain relaxation or allows some rearrangements of PS molecules in the residual layer. This assumption is in agreement with the results of Gin *et al.*,[24] who reported that the inner flattened layer has no thermal expansion when the loosely attached layer is thick, whereas after removing the outer loosely adsorbed chains the flattened layer can reorganize due to the resultant empty spaces (*i.e.*, more free volume). Toluene diffuses easily into the flattened layer during rinsing. It acts as a plasticizer, lowering the T_g below room temperature.[9,42] Hence the molecular mobility of the PS chains increases by minimizing the cumulative intermolecular forces along the chains, leading to a reduction in the cohesion. Thus, PS chains can glide over one another in the presence of toluene solvent to reach equilibrium by releasing the residual stress and/or erasing the density variations imposed during the spin-coating process.

CONCLUSION

In conclusion, our results show that a two-step top-down approach consisting (1) in the preparation of homogeneous thick films by spin-coating and (2) in thinning them by rinsing in a good solvent (*e.g.*, toluene) could solve one of the most mysterious unanswered questions encountered in the physics of extremely confined polymer films: why are ultrathin

films of PS unstable on oxide-free silicon surfaces? We first demonstrated that the leaching procedure was perfectly adapted to obtain thin and smooth residual films without any holes even after postannealing above T_g. By varying two parameters, such as rinsing time (t_{rins}) and preannealing time (t_{an}), several desired thicknesses were obtained below 7 nm. After postannealing above T_g, we observed that residual films deposited on oxide-free H-Si surfaces do not dewet as expected from the van der Waals theory. On the contrary, films deposited on SiO_x-Si substrates with a SiO_x layer thickness around 2 nm showed a spinodal dewetting below a critical film thickness h_{trans} of about ~2.9 nm. Above this value films are in a metastable state and were found to be uniform on a time scale of a few months. This transition between the two regimes, unstable and metastable, is in perfect agreement with the intermolecular van der Waals interactions theory. We attribute the stability of the films deposited on oxide-free silicon to the capability of toluene to remove either the residual stresses of the film or the density variations inside the film.

METHODS

Preparation of Substrate Surfaces. We adopted HF and RCA treatments of Si(001) prior to depositing polymer films. These two treatments were chosen to make oxide-free (in H-Si) and freshly native-oxide-covered (in SiO_x-Si) Si surfaces. HF treatment was done by immerging Si wafers (of size ~15 × 15 mm^2) in a solution of hydrogen fluoride (HF, Merck, 10%) for 3 min at room temperature (25 °C). This resulted in oxide-free hydrophobic H-terminated Si substrates. In RCA cleaning, the Si surfaces (of size ~15 × 15 mm^2) were made hydrophilic by immerging them in a mixed solution of ammonium hydroxide (NH_4OH, Sigma-Aldrich, 25%), hydrogen peroxide (H_2O_2, Acros Organics, 35%), and Milli-Q water ($H_2O/NH_4OH/H_2O_2$ = 2:1:1, by volume) for 10 min at 100 °C. This solution is designed to remove organic contaminants by both the solvating action of the NH_4OH and the oxidizing action of the H_2O_2. The oxidizing agent H_2O_2 forms a continuous, thin silicon oxide (SiO_x) layer on the substrate surface. The thickness of this oxide layer is expected to be ~2 nm,[43] similar to that of the piranha treatment.[30] Then the substrates were thoroughly rinsed with water and dried prior to spin-coating. The evidence of the 2 nm oxide layer and its complete removal due to RCA and HF cleaning, respectively, is obtained from X-ray photoelectron spectroscopy (XPS) and XRR (see Supporting Information Figure S10).

Preparation of Polystyrene Ultrathin Films. PS thin films (Polymer Source, M_w = 1.36 × 10^5 g/mol, R_g ≈ 13.6 nm, polydispersity M_w/M_n = 1.05) of initial thickness varying from ~3 to 130 nm were prepared by adjusting the concentration of PS/toluene solutions. Films were deposited by spin-coating (Karl Suss and spinNXG-M1) these solutions at 2000 rpm for 1 min onto both HF-treated (designated as H-Si) and RCA-treated (designated as SiO_x-Si) Si substrates. Selected films were preannealed at 160 °C during 24 h under vacuum (~10^{-3} mbar). Then we switched off the oven, and the samples were cooled naturally until the temperature reached 25 °C under vacuum. Residual films were postannealed at 120 °C following the same protocol. We also prepared another three films of thickness 7 nm on the SiO_x-Si substrate having different molecular weights, *i.e.*, 0.13 × 10^5 g/mol (R_g ≈ 3 nm), 0.29 × 10^5 g/mol (R_g ≈ 5 nm), and 2.21 × 10^5 g/mol (R_g ≈ 18 nm).

Solvent Rinsing Process. The toluene rinsing of the spin-coated polymer films was carried out in a systematic way by immerging the films every 10 min in 100 mL of toluene at ambient temperature. The rinsing procedure was operated as followed: (1) films were put vertically inside a beaker filled with toluene; (2) they were then kept for the desired time under toluene; (3) they were vertically withdrawn from the solution; (4) a mild flow of N_2 was then applied on the surface of the film to remove the remaining toluene. This procedure was repeated several times on each film. Their thicknesses at each time were measured by X-ray reflectivity and sometimes cross verified by ellipsometry (Sentech, SE850).

X-ray Reflectivity. Specular X-ray reflectivity was used to characterize the thickness and quality of the spin-coated and toluene-rinsed films. XRR measurements were carried out using a versatile X-ray reflectometer. The diffractometer (Empyrean Panalytical) was equipped with a Cu source (sealed tube) followed by a W/C mirror to select and enhance Cu Kα radiation (λ = 1.543 Å). All measurements were carried out in symmetric $\theta-\theta$ geometry, in which the sample was kept fixed during the measurements. The intensity was measured with a Pixel 3D detector using a fixed aperture of three channels (0.165°) in the 2θ direction. Under such conditions, at a given angle of incidence θ, a nonvanishing wave vector component, q_z, is given by $(4\pi/\lambda)\sin\theta$ with resolution 0.0014 $Å^{-1}$. XRR essentially provides an electron density profile, *i.e.*, average electron density (ρ) in-plane ($x-y$) as a function of depth (z). From the EDP, it is possible to estimate the film thickness, the electron density, and the interfacial roughness. Analysis of XRR data has been carried out using the matrix technique.[45] For the analysis, the film is divided into a number of slabs including roughness at each interface. An instrumental resolution in the form of a Gaussian function and a constant background were also included in the data analysis. Indeed it was observed that the diffuse scattering measured by off-specular scans was negligible over most of the measured q range. The diffuse scattering was merging with the true specular reflectivity at high q_z, justifying the use of a constant background in the data analysis. Here, as we are dealing with ultrathin films thinner than ~10 nm that give rise to a very small number of oscillations before reaching the background, a large error of 0.5 nm in the estimation of thickness is possible.

Atomic Force Microscopy. The surface morphology of the films was collected through an Agilent 5500 AFM in intermittent-contact mode in air (Nanosensor PPP-NCHR-W tip), and scans were performed over several portions of the films. WSxM software was used for image processing and analysis.[46]

Attenuated Total Reflectance. The absorbance study was performed by ATR at the SMIS synchrotron beamline of Soleil. Samples were analyzed by infrared absorption spectroscopy using multiple internal reflection at ambient conditions. Films used for these measurements were deposited on 0.5 mm × 10 mm × 30 mm Si wafers having 45° bevels on the edges. IR radiation from an interferometer was focused at normal incidence onto one of the two bevels of the sample. Then it propagated through the sample after reflecting internally about 60 times.

Conflict of Interest: The authors declare no competing financial interest.

Supporting Information Available: Additional experimental details and figures. The Supporting Information is available free of charge on the ACS Publications website at DOI: 10.1021/acsnano.5b02381.

Acknowledgment. We gratefully acknowledge the CEFIPRA/IFCPAR program and Région des Pays de la Loire for financial support. We would like to thank Kenza Ayche for AFM imaging of a few samples. J.K.B. thankfully acknowledges the Department of Science and Technology (DST), Government of India, for providing a research grant through the INSPIRE Faculty Award (IFA13-PH-79). We thank Paul Dumas for his help in ATR measurements at SMIS beamline of Soleil. Experiment planning and performance: J.K.B., T.B., A.G., and A.B.U.; subject initiation: G.V.; theoretical

calculations: T.B.; AFM measurements and analysis: N.D. and J.K. B.; sample preparation and XRR analysis: J.K.B., T.B., and M.S.C.; manuscript written by J.K.B., T.B., A.G., and G.V. and edited by N. D., A.B.U., E.A.C., M.S.C., and Y.G.

REFERENCES AND NOTES

1. Adhikari, B.; Majumdar, S. Polymers in Sensor Applications. *Prog. Polym. Sci.* **2004**, *29*, 699–766.
2. Huang, Q.; Yoon, I.; Villanueva, J.; Kim, K.; Sirbuly, D. J. Quantitative Mechanical Analysis of Thin Compressible Polymer Monolayers on Oxide Surfaces. *Soft Matter* **2014**, *10*, 8001–8010.
3. Lee, L.-H. *Adhesive Bonding*; Plenum Press, 1991.
4. Hook, A. L.; Chang, C.-Y.; Yang, J.; Luckett, J.; Cockayne, A.; Atkinson, S.; Mei, Y.; Bayston, R.; Irvine, D. J.; Langer, R.; Anderson, D. G.; Williams, P.; Davies, M. C.; Alexander, M. R. Combinatorial Discovery of Polymers Resistant to Bacterial Attachment. *Nat. Biotechnol.* **2012**, *30*, 868–875.
5. Günes, S.; Neugebauer, H.; Sariciftci, N. S. Conjugated Polymer-Based Organic Solar Cells. *Chem. Rev.* **2007**, *107*, 1324–1338.
6. Li, G.; Zhu, R.; Yang, Y. Polymer Solar Cells. *Nat. Photonics* **2012**, *6*, 153–161.
7. Kim, C.; Facchetti, A.; Marks, T. J. Polymer Gate Dielectric Surface Viscoelasticity Modulates Pentacene Transistor Performance. *Science* **2007**, *318*, 76–80.
8. Bollinne, C.; Cuenot, S.; Nysten, B.; Jonas, A. M. Spinodal-Like Dewetting of Thermodynamically-Stable Thin Polymer Films. *Eur. Phys. J. E: Soft Matter Biol. Phys.* **2003**, *12*, 389–396.
9. Reiter, G.; Hamieh, M.; Damman, P.; Sclavons, S.; Gabriele, S.; Vilmin, T.; Raphael, E. Residual Stresses in Thin Polymer Films Cause Rupture and Dominate Early Stages of Dewetting. *Nat. Mater.* **2005**, *4*, 754–758.
10. Napolitano, S.; Wübbenhorst, M. The Lifetime of the Deviations from Bulk Behaviour in Polymers Confined at the Nanoscale. *Nat. Commun.* **2011**, *2*, 260−1−7.
11. Brochard-Wyart, F.; Di Meglio, J. M.; Quére, D.; De Gennes, P. G. Spreading of Nonvolatile Liquids in a Continuum Picture. *Langmuir* **1991**, *7*, 335–338.
12. Israelachvili, J. N. *Intermolecular and Surface Forces*; revised third ed.; Academic Press, 2011.
13. Sharma, A.; Reiter, G. Instability of Thin Polymer Films on Coated Substrates: Rupture, Dewetting, and Drop Formation. *J. Colloid Interface Sci.* **1996**, *178*, 383–399.
14. Visser, J. On Hamaker Constants: A Comparison Between Hamaker Constants and Lifshitz-van der Waals Constants. *Adv. Colloid Interface Sci.* **1972**, *3*, 331–363.
15. Hough, D. B.; White, L. R. The Calculation of Hamaker Constants from Liftshitz Theory with Applications Applications to Wetting Phenomena. *Adv. Colloid Interface Sci.* **1980**, *14*, 3–42.
16. Van Oss, C. J.; Chaudhury, M. K.; Good, R. J. Interfacial Lifshitz-van der Waals and Polar Interactions in Macroscopic Systems. *Chem. Rev.* **1988**, *88*, 927–942.
17. Kerle, T.; Yerushalmi-Rozen, R.; Klein, J.; Fetters, L. van der Waals Stable Thin Liquid Films: Correlated Undulations and Ultimate Dewetting. *Europhys. Lett.* **1998**, *44*, 484–490.
18. Ackler, H. D.; French, R. H.; Chiang, Y.-M. Comparisons of Hamaker Constants for Ceramic Systems with Intervening Vacuum or Water: from Force Laws and Physical Properties. *J. Colloid Interface Sci.* **1996**, *179*, 460–469.
19. Bergström, L. Hamaker Constants of Inorganic Materials. *Adv. Colloid Interface Sci.* **1997**, *70*, 125–169.
20. Zhao, H.; Wang, Y. J.; Tsui, O. K. Dewetting Induced by Complete *versus* Nonretarded van der Waals Forces. *Langmuir* **2005**, *21*, 5817–5824.
21. Seemann, R.; Herminghaus, S.; Jacobs, K. Dewetting Patterns and Molecular Forces: A Reconciliation. *Phys. Rev. Lett.* **2001**, *86*, 5534–5537.
22. Sharma, A.; Mittal, J.; Verma, R. Instability and Dewetting of Thin Films Induced by Density Variations. *Langmuir* **2002**, *18*, 10213–10220.
23. Xue, L.; Han, Y. Inhibition of Dewetting of Thin Polymer Films. *Prog. Mater. Sci.* **2012**, *57*, 947–979.
24. Gin, P.; Jiang, N.; Liang, C.; Taniguchi, T.; Akgun, B.; Satija, S. K.; Endoh, M. K.; Koga, T. Revealed Architectures of Adsorbed Polymer Chains at Solid-Polymer Melt Interfaces. *Phys. Rev. Lett.* **2012**, *109*, 265501−1–5.
25. Jiang, N.; Shang, J.; Di, X.; Endoh, M. K.; Koga, T. Formation Mechanism of High-Density, Flattened Polymer Nanolayers Adsorbed on Planar Solids. *Macromolecules* **2014**, *47*, 2682–2689.
26. Fujii, Y.; Yang, Z.; Leach, J.; Atarashi, H.; Tanaka, K.; Tsui, O. K. C. Affinity of Polystyrene Films to Hydrogen-Passivated Silicon and Its Relevance to the T_g of the Films. *Macromolecules* **2009**, *43*, 7428–7432.
27. Guiselin, O. Irreversible Adsorption of A Concentrated Polymer Solution. *Europhys. Lett.* **1992**, *17*, 225–230.
28. Johnson, H. E.; Granick, S. New Mechanism of Nonequilibrium Polymer Adsorption. *Science* **1992**, *255*, 966–968.
29. Priestley, R. D.; Ellison, C. J.; Broadbelt, L. J.; Torkelson, J. M. Structural Relaxation of Polymer Glasses at Surfaces, Interfaces, and in Between. *Science* **2005**, *309*, 456–459.
30. Van der Lee, A.; Hamon, L.; Holl, Y.; Grohens, Y. Density Profiles in Thin PMMA Supported Films Investigated by X-ray Reflectometry. *Langmuir* **2001**, *17*, 7664–7669.
31. Vignaud, G.; Chebil, M. S.; Bal, J. K.; Delorme, N.; Beuvier, T.; Grohens, Y.; Gibaud, A. Densification and Depression in Glass Transition Temperature in Polystyrene Thin Films. *Langmuir* **2014**, *30*, 11599–11608.
32. Bal, J. K.; Beuvier, T.; Chebil, M. S.; Vignaud, G.; Grohens, Y.; Sanyal, M. K.; Gibaud, A. Relaxation of Ultrathin Polystyrene Films Hyperswollen in Supercritical Carbon Dioxide. *Macromolecules* **2014**, *47*, 8738–8747.
33. Housmans, C.; Sferrazza, M.; Napolitano, S. Kinetics of Irreversible Chain Adsorption. *Macromolecules* **2014**, *47*, 3390–3393.
34. Bal, J.; Kundu, S.; Hazra, S. Growth and Stability of Langmuir-Blodgett Films on OH-, H-, or Br-Terminated Si (001). *Phys. Rev. B: Condens. Matter Mater. Phys.* **2010**, *81*, 045404−1–8.
35. Jabbari, E.; Peppas, N. A. Use of ATR-FTIR to Study Interdiffusion in Polystyrene and Poly (vinyl methyl ether). *Macromolecules* **1993**, *26*, 2175–2186.
36. Becker, J.; Grün, G.; Seemann, R.; Mantz, H.; Jacobs, K.; Mecke, K. R.; Blossey, R. Complex Dewetting Scenarios Captured by Thin-Film Models. *Nat. Mater.* **2003**, *2*, 59–63.
37. Vrij, A. Possible Mechanism for the Spontaneous Rupture of Thin, Free Liquid Films. *Discuss. Faraday Soc.* **1966**, *43*, 23–33.
38. Xie, R.; Karim, A.; Douglas, J.; Han, C.; Weiss, R. Spinodal Dewetting of Thin Polymer Films. *Phys. Rev. Lett.* **1998**, *81*, 1251–1254.
39. Reiter, G.; De Gennes, P. Spin-Cast, Thin, Glassy Polymer Films: Highly Metastable Forms of Matter. *Eur. Phys. J. E: Soft Matter Biol. Phys.* **2001**, *6*, 25–28.
40. Seemann, R.; Herminghaus, S.; Jacobs, K. Gaining Control of Pattern Formation of Dewetting Liquid Films. *J. Phys.: Condens. Matter* **2001**, *13*, 4925–4938.
41. Reiter, G.; Khanna, R.; Sharma, A. Enhanced Instability in Thin Liquid Films by Improved Compatibility. *Phys. Rev. Lett.* **2000**, *85*, 1443–1445.
42. Xu, L.; Sharma, A.; Joo, S. W. Dewetting of Stable Thin Polymer Films Induced by a Poor Solvent: Role of Polar Interactions. *Macromolecules* **2012**, *45*, 6628–6633.
43. Al-Bayati, A. H.; Orrman-Rossiter, K. G.; van den Berg, J. A.; Armour, D. G. Composition and Structure of the Native Si Oxide by High Depth Resolution Medium Energy Ion Scattering. *Surf. Sci.* **1991**, *241*, 91–102.
44. Bal, J. K.; Kundu, S.; Hazra, S. Hydrophobic to Hydrophilic Transition of HF-Treated Si Surface During Langmuir−Blodgett Film Deposition. *Chem. Phys. Lett.* **2010**, *500*, 90–95.
45. Gibaud, A.; Vignaud, G. In *X-ray and Neutron Reflectivity*; Daillant, J., Gibaud, A., Eds.; Springer: Berlin, Germany, 2009; Lecture Notes in Physics 770, pp 85−131.
46. Horcas, I.; Fernandez, R.; Gomez-Rodriguez, J. M.; Colchero, J.; Gomez-Herrero, J.; Baro, A. M. WSXM: a Software for Scanning Probe Microscopy and a Tool for Nanotechnology. *Rev. Sci. Instrum.* **2007**, *78*, 014205–1.